Region of interest-bounded COVID-19 lung screening using images from portable X-ray devices *

Plácido L. Vidal[12], Joaquim de Moura[12], Lucía Ramos[12], Jorge Novo[12], and Marcos Ortega[12]

[1] Centro de investigación CITIC, Universidade da Coruña, A Coruña, Galicia, Spain.
[2] Grupo VARPA, INIBIC, Universidade da Coruña, A Coruña, Galicia, Spain.
(placido.francisco.lizancos.vidal, joaquim.demoura, l.ramos, jnovo, mortega)@udc.es

Abstract

X-ray analysis of the lungs was the main method to assess the degree of affliction of SARS-COV-2. Due to the high contagiousness of this pathology, this assessment was conducted using portable X-ray devices. Automatic methodologies were proposed to compensate the image quality of said portable X-ray devices. However, these methodologies were shown to be exploiting external information (such as pacemakers or ventilators present in the images) to determine the severity. For this reason, we present a methodology specially designed to reduce the effect on an automatic methodology of these extraneous artifacts. We extract the lung region and we perform a screening of the presence of the pathology using only the pulmonary region. Finally, to ascertain the performance of the system (and provide explainability to the clinical experts), we generate the corresponding activation maps. The presented methodology has achieved a more than satisfactory performance in all the scenarios and the activation maps clearly indicate that the system is successfully using information from the lung region while excluding elements unrelated to the disease.

1 Introduction

During the COVID-19 pandemic, the diagnosis was performed in specific isolated circuits due to its contagiousness. Given the saturated healthcare services and the extenuating shifts in hospitals, automated methodologies were proposed to palliate the error derived from subjectivity. However, said analyses were mainly conducted using portable X-ray devices, which can be conveniently deployed in these circuits at the cost of limited versatility of capture planes and consequent lesser quality of the images. For this reason, the aforementioned methodologies were also adapted to specifically work under these challenging scenarios [1].
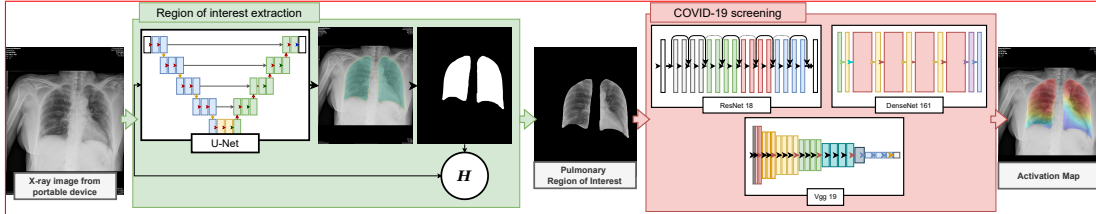
Figure 1: Stages of the proposed methodology.

In general, these methodologies were shown to be exploiting information external to the explicit domain of the pathology rather than its own biological artifacts. These systems were taking advantage of data like the presence of medical equipment and other extraneous factors outside the lung region of the patient that could indicate the presence of symptoms or pathologies (increasing the perceived risk and/or severity of the pathology) [2]. For this reason, in this work we present a two-stage methodology specially designed for COVID-19 screening in these complex scenarios, as well as the generation of activation maps that indicate the attention of the network in the original input images to provide the clinical experts an extra layer of explainability.

2   Methodology

Our methodology is divided into two main steps. In the first step, we use a methodology that is robust to the artifacts, structures and deformations commonly present in portable chest radiographs. We use a proposal based on the work of Vidal *et al.* [3], a double-stage transfer learning approach where, from different medical domains, the model is trained to properly segment radiographs from portable devices. Then, we perform the Hadarmard product (H) between the original input image and the resulting segmentation. This way, the information passed to the second stage only contains patterns from the pulmonary region of the images.

In the second stage, we train three networks (a Vgg19, Resnet18 and DenseNet161) to evaluate the performance in three different scenarios. In the first scenario, we evaluate the model to distinguish normal images from any kind of pulmonary pathology (included COVID-19). In the second scenario, we train the model to discern COVID-19 images from any other type (both normal and pathological). Finally, in the third scenario, we evaluate the performance of the model independently for each class.

3   Results

The dataset employed in this work was composed by a total of 2,071 radiographs from portable devices. These images were obtained from patients that were diagnosed with COVID-19, pathologies with similar features and patients with normal lungs. 716 images were randomly selected from each category to compose the final dataset. These images were acquired with an Agfa dr100E GE and Optima Rx200 portable X-ray devices by the radiology service of the Complexo Hospitalario Universidario de A Coruña (CHUAC). The test results for each of the experiments are presented in Table 1. As the reader can see, while in the case for normal vs. the rest the Vgg19 architecture obtained better results than the other two models, the DenseNet161 model is the one that, overall, performed the best. Moreover, in this same scenario where the Vgg19 bested the other architectures, the DenseNet161 obtained close results to it, inside the

Table 1: Best test results for the experiments evaluating the different combinations of healthy (H), pathological (P) and COVID-19 (C) classes.

Architecture	Accuracy	Class	Precision	Recall	F1–Score
Vgg19	89.6% ± 1.29%	**H**	87.6% ± 1.74%	91.8% ± 1.72%	89.8% ± 1.47%
		P+C	91.8% ± 1.83%	87.4% ± 1.36%	89.6% ± 1.29%
DenseNet161	94.7% ± 1.34%	**H+P**	93.0% ± 1.10%	99.4% ± 0.80%	96.0% ± 1.10%
		C	98.4% ± 2.24%	86.4% ± 2.42%	91.8% ± 1.94%
DenseNet161	83.4% ± 2.06%	**H**	77.2% ± 4.07%	81.4% ± 3.38%	79.2% ± 2.99%
		P	80.4% ± 3.88%	78.8% ± 4.12%	79.4% ± 2.73%
		C	93.8% ± 2.64%	90.2% ± 1.72%	91.8% ± 0.40%

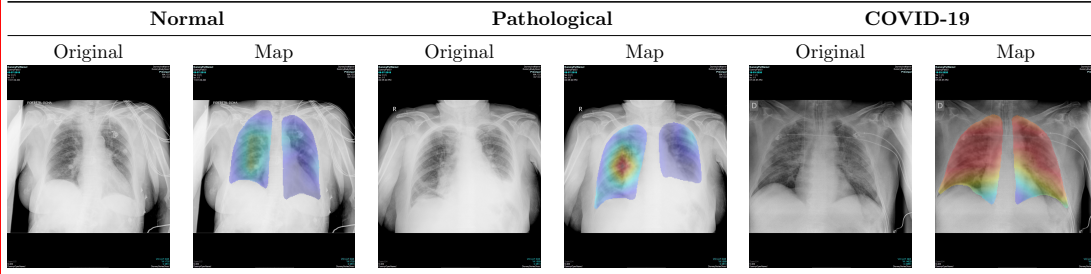| Normal		Pathological		COVID-19	
Original	Map	Original	Map	Original	Map

Figure 2: Random examples of maps generated for each of the considered categories for the three-class approach and DenseNet161 architecture.

range of its standard deviation. Nonetheless, in all the presented combinations all the models are able to successfully discern the presented scenarios. In fact, as shown in the three-class approach, they perform the best with the COVID-19 class. This is possibly due to the fact that it is a very defined group, while the pathological class in general is a more heterogeneous scenario (as mentioned, including images from pathologies with similar marks as COVID-19).

Finally, a random selection of the maps generated by our proposal for each class is shown in Figure 2. In these maps, we can see how the network tends to focus on the shape, extension and texture of the darkest regions of the pulmonary region. Moreover, overall, the COVID-19 maps tend to present a more intense and widespread detection than the other two scenarios.

4   Conclusions

The methodology presented in this work is able to successfully determine the presence or absence of COVID-19 in radiographs from portable devices (despite even against images with pathologies similar to COVID-19, like other viral and bacterial pneumonias). Additionally, the activation maps represent an extra aide and explainability layer for clinicians to study. As future works, we plan to further analyze and understand the features indicated by the maps, as well as to adapt our proposal to other domains in similar situations.

References

[1] Joaquim de Moura, Lucía Ramos García, Plácido L. Vidal, Milena Cruz, Laura Abelairas López, Eva Castro Lopez, Jorge Novo, and Marcos Ortega. Deep convolutional approaches for the analysis of covid-19 using chest x-ray images from portable devices. *IEEE Access*, 8:195594–195607, 2020.

[2] Plácido L Vidal, Joaquim de Moura, Jorge Novo, and Marcos Ortega. Pulmonary-restricted COVID-19 informative visual screening using chest x-ray images from portable devices. In *Image Analysis and Processing – ICIAP 2022*, Lecture notes in computer science, pages 65–76. Springer International Publishing, Cham, 2022.

[3] Plácido L Vidal, Joaquim de Moura, Jorge Novo, and Marcos Ortega. Multi-stage transfer learning for lung segmentation using portable x-ray devices for patients with COVID-19. *Expert Syst. Appl.*, 173(114677):114677, July 2021.